

## The Curie temperature distribution of FePt granular magnetic recording media

O. Hovorka, S. Devos, Q. Coopman, W. J. Fan, C. J. Aas et al.

Citation: *Appl. Phys. Lett.* **101**, 052406 (2012); doi: 10.1063/1.4740075

View online: <http://dx.doi.org/10.1063/1.4740075>

View Table of Contents: <http://apl.aip.org/resource/1/APPLAB/v101/i5>

Published by the [American Institute of Physics](http://www.aip.org).

---

### Related Articles

Influence of the magnetic field on the plasmonic properties of transparent Ni anti-dot arrays  
*Appl. Phys. Lett.* **101**, 063107 (2012)

Large half-metallic gap in ferromagnetic semi-Heusler alloys CoCrP and CoCrAs  
*Appl. Phys. Lett.* **101**, 062402 (2012)

Micro-dent arrays fabricated by a novel net mask laser shock processing on the surface of LY2 aluminum alloy  
*J. Appl. Phys.* **112**, 023117 (2012)

Variation of magnetic domain structure during martensite variants rearrangement in ferromagnetic shape memory alloys  
*Appl. Phys. Lett.* **101**, 032401 (2012)

Anomalous low temperature stair like coercivity decrease due to magnetostatic coupling between superconducting and ferromagnetic particles in mixed powders  
*J. Appl. Phys.* **112**, 013912 (2012)

---

### Additional information on *Appl. Phys. Lett.*

Journal Homepage: <http://apl.aip.org/>

Journal Information: [http://apl.aip.org/about/about\\_the\\_journal](http://apl.aip.org/about/about_the_journal)

Top downloads: [http://apl.aip.org/features/most\\_downloaded](http://apl.aip.org/features/most_downloaded)

Information for Authors: <http://apl.aip.org/authors>

## ADVERTISEMENT

**AEROTECH**  
nano Motion Technology

Click here for the **FREE**  
nano Motion Technology Catalog

Linear Single-Axis and Dual-Axis Stages

Rotary Stages

Goniometers

Vertical Lift and Z Stages

The advertisement features a blue background with a white wave-like pattern at the bottom. It displays four categories of motion control products: Linear Single-Axis and Dual-Axis Stages, Rotary Stages, Goniometers, and Vertical Lift and Z Stages. Each category is accompanied by images of the respective hardware. On the right side, there is a vertical image of the 'nano Motion Technology' catalog, which includes a list of features: Long Travel, High Dynamic Performance, High Accuracy, High Resolution, and Easy-to-Use Software.

# The Curie temperature distribution of FePt granular magnetic recording media

O. Hovorka,<sup>1,a)</sup> S. Devos,<sup>1</sup> Q. Coopman,<sup>1</sup> W. J. Fan,<sup>1</sup> C. J. Aas,<sup>1</sup> R. F. L. Evans,<sup>1</sup> Xi Chen,<sup>2</sup> G. Ju,<sup>2</sup> and R. W. Chantrell<sup>1</sup>

<sup>1</sup>Department of Physics, The University of York, York YO10 5DD, United Kingdom

<sup>2</sup>Seagate Technology, 47010 Kato Road, Fremont, California 94538, USA

(Received 20 April 2012; accepted 17 July 2012; published online 1 August 2012)

We present atomistic calculations of the magnetic phase transition behavior in an L1<sub>0</sub> FePt system to study the effect of grain size distribution on the Curie temperature ( $T_c$ ) dispersion with relevance to heat assisted magnetic recording. Identifying the relation between the size and  $T_c$  of a grain by means of finite size scaling analysis of the differentiated magnetization versus  $T$  data allows to show that a lognormal size distribution transforms into a lognormal  $T_c$  distribution with moments dependent on the critical exponents. We also address the question of the universality class of FePt.

© 2012 American Institute of Physics. [<http://dx.doi.org/10.1063/1.4740075>]

Heat assisted magnetic recording (HAMR)<sup>1–4</sup> is the most likely candidate technology to achieve recording densities significantly beyond those accessible to conventional perpendicular magnetic recording. The recently announced demonstration of a density of 1 Tbit/in<sup>2</sup> brings a transition to HAMR technology a step closer. An advantage of HAMR, noted in Ref. 1, is the fact that requirements of increasing head field gradients, which limit achievable areal densities in conventional perpendicular recording, are reduced by the large temperature gradients produced by the laser heating. However, in order to maximize the effect the rate of change of magnetization with temperature,  $dM/dT$ , must also be high, suggesting recording close to the Curie temperature  $T_c$ . This implies the necessity to understand static and dynamic magnetic behavior near  $T_c$  such as, for example, the recently predicted linear reversal mechanism<sup>5,6</sup> or the influence of grain size distribution  $f_D(D)$  on the  $T_c$  dispersion  $f_T(T_c)$ —the understanding of which will be the main subject of the present work. Indeed, uncontrolled  $f_T(T_c)$  may result in smeared  $M(T)$  dependence and thus reduced  $dM/dT$  near  $T_c$ , and as such is a crucial factor with a potentially detrimental effect on HAMR.

The approach undertaken here to relate  $f_D(D)$  and  $f_T(T_c)$  relies on exploring the critical behavior in magnetic grains of variable size  $D$ . The task is to quantify the size dependence of the Curie temperature,  $T_c(D)$ , extracted from  $M(T)$  data computed from an atomistic model of ordered ferromagnetic FePt (Fig. 1(a)), which is, with its low bulk Curie temperature  $T_c^\infty$  and large anisotropy constant  $K$ ,<sup>7,8</sup> currently regarded as the best candidate material for HAMR media. The  $T_c(D)$  dependence is expected to follow the finite size scaling law:

$$\epsilon_c(D) = \frac{T_c^\infty - T_c(D)}{T_c^\infty} = \left(\frac{d_0}{D}\right)^\lambda, \quad (1)$$

where  $\lambda$  is the so-called phenomenological shift exponent and  $d_0$  is the microscopic length scale close to the dimension of a

single unit cell in the lattice structure of the material, see, e.g., Refs. 9–11. The exponent  $\lambda$  is related to the correlation length universal critical exponent  $\nu$  to be defined below and it is expected that  $\lambda \leq \nu^{-1}$  depending on the nature of the experiment;<sup>12,13</sup>  $\lambda = \nu^{-1}$  in the absence of higher order system size effects, which will be shown to be the case also here.

Given only limited studies of size dependent critical behavior of FePt,<sup>11,14</sup> available critical parameters are insufficient for careful comparison with our study. Therefore, we consider two different models: an FePt effective Hamiltonian with a long-range exchange (LE) term derived from density functional theory (DFT) calculations,<sup>8</sup> and a "test" model with the nearest neighbor exchange (NE), which is expected to closely resemble the critical behavior of the well studied Heisenberg model<sup>15</sup> and thus allows validation of the present approach. Thereby we demonstrate that because of LE interaction, FePt may not belong to the universality class of the NE Heisenberg model, giving rise to a weaker variation of  $T_c$  with  $D$  according to Eq. (1). Equation (1) also allows relating  $f_T(T_c)$  to  $f_D(D)$ , and we show analytically that the realistic choice of lognormal distribution  $f_D(D)$  leads precisely to the lognormal form of  $f_T(T_c^\infty - T_c)$ .

The LE atomistic model used in the present study utilizes an effective Hamiltonian of FePt parametrized based on DFT calculations,<sup>8</sup> which is of the form

$$\mathcal{H} = -\sum_{i \neq j} (J_{ij} \mathbf{S}_i \cdot \mathbf{S}_j + K_{ij} S_i^z S_j^z) - \sum_i K_i (S_i^z)^2, \quad (2)$$

where  $J_{ij}$  is effective exchange (considered long-ranged as its range extends beyond five lattice spacings), and  $K_i$  and  $K_{ij}$  are, respectively, the effective uniaxial single-ion and two-ion anisotropy contributions defined in more detail in Ref. 8. The NE Hamiltonian is obtained from Eq. (2) by specifying a nearest neighbor only exchange  $J_{ij} = 3.0^{-21}$  J/link and by setting  $K_{ij} = 0$ . The anisotropy term  $K_i$  remains included. In both NE and LE Hamiltonians, the spin moments are expressed as unit vectors  $\mathbf{S}_i = \mu_i / |\mu_i|$ . The system is integrated using the Landau-Lifshitz-Gilbert equation with the Langevin Dynamics formalism.<sup>16,17</sup> The system is integrated using the Heun numerical scheme and a timestep

<sup>a)</sup>Electronic mail: [ondrej.hovorka@york.ac.uk](mailto:ondrej.hovorka@york.ac.uk).

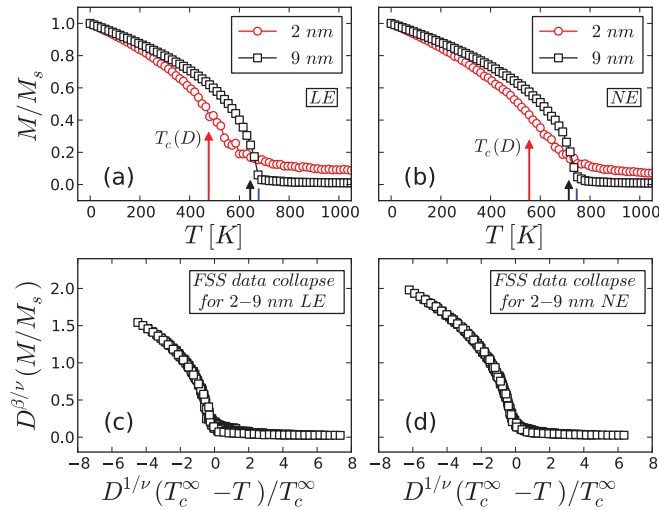


FIG. 1. (a) Computed  $M$  vs  $T$  data for LE FePt model and (b) nearest NE model, for 2 nm and 9 nm grains. Vertical arrows indicate finite size Curie temperatures  $T_c(D)$  determined as minima of  $\Delta M/\Delta T$  vs  $T$  for every grain size  $D$  (also in Fig. 2). The vertical line corresponds to the bulk  $T_c^\infty$  listed in Table I. (c) A scaling collapse according to Eq. (3) for LE and (d) NE models, including grain sizes 2, 3, ..., 9 nm and critical parameters  $T_c^\infty$ ,  $\nu$ , and  $\beta$  summarised in Table I.

of  $1.0 \times 10^{-15}$  s. Since we are interested only in equilibrium properties we set the precessional damping constant  $\alpha = 1.0$  for computational efficiency. Simulated samples were cut from a bulk crystal in the shape of a cylinder with diameter  $D$  and height  $D$  varying in the range 2 nm to 9 nm in 1 nm increments. The system for every  $D$  was equilibrated at each temperature for 20 000 time steps and then a thermodynamic average magnetization calculated over further 20 000 time steps. Examples of  $M(T)$  data computed in this way for  $D = 2, 9$  nm for LE FePt and NE models are shown Figs. 1(a) and 1(b), respectively.

In general terms, the behavior of a bulk system near its Curie temperature  $T_c^\infty$  is described by divergent tendencies of some of its thermodynamic variables.<sup>15</sup> For example, the correlation length  $\xi$  which quantifies the extent of magnetic ordering in a system is expected to follow a power law divergence  $\xi \sim d_0 |\epsilon|^{-\nu}$  where the reduced temperature is defined as  $\epsilon = (T_c^\infty - T)/T_c^\infty$  similarly to the critical  $\epsilon_c$  introduced in Eq. (1), and  $\nu$  is the correlation length universal critical exponent. Other characteristics approach a finite value as  $T \rightarrow T_c^\infty$ . For example, the magnetization  $M$  approaches zero following a power law with the “magnetization” universal critical exponent  $\beta$ :  $M \sim |\epsilon|^\beta$ . Strictly speaking, such non-analytic behaviors exist only in the thermodynamic limit. Thermodynamic quantities for systems with some characteristic dimensions  $D$  finite are always rounded, shifted, and smeared out, and as a result, the critical region becomes hard to access. These difficulties appear as soon as the correlation length  $\xi$  becomes comparable with the smallest characteristic dimension  $D$ , i.e.,  $\xi \sim D$  or equivalently  $d_0 |\epsilon|^{-\nu} \sim D$ , which directly implies a shift of the size-dependent  $T_c(D)$  away from the bulk value  $T_c^\infty$ , thus motivating the phenomenological Eq. (1).

This behavior is demonstrated in Figs. 1(a) and 1(b) where in both cases of LE FePt and NE models, the reduction of the finite size  $T_c(D)$  from the bulk  $T_c^\infty$  becomes

more pronounced for small 2 nm grains. Figure 2 further confirms this systematic trend for grains of diameters in the range 2, ..., 9 nm. As conventional in experiments, e.g., Refs. 10 and 11, we determined the finite size  $T_c(D)$  as corresponding to the minimum of derivative  $\Delta M/\Delta T$  as illustrated in the inset for a 3 nm grain. Figure 2 shows that the variation of  $T_c(D)$  is slightly weaker for the LE FePt model than for the NE model, which suggests a difference between the shift exponents  $\lambda$ . This issue will be addressed below. To apply Eq. (1) to the data in Fig. 2, it is first necessary to identify the bulk  $T_c^\infty$  which, although often readily accessible in experiments, is hard to access in computations.

To extrapolate the finite size computational data to the thermodynamic limit to identify the bulk  $T_c^\infty$ , we utilize the finite system size scaling (FSS) analysis.<sup>18,19</sup> The FSS method allows, in addition to  $T_c^\infty$ , a direct extraction of critical exponents  $\nu$  and  $\beta$ . It is based on the concept of universality,<sup>19</sup> which in the context of the present study implies (1) independence of universal critical exponents on  $D$  and (2) data similarity near the critical point, i.e., that after rescaling the  $M(T)$  data for all different  $D$  by the same appropriate combinations of critical exponents and non-universal parameters, they will all collapse onto a universal curve which we denote as  $y = \tilde{M}(x)$ . Specifically, the FSS scaling theory for the one-dimensional scaling relevant to the present study gives the following FSS scaling ansatz when expressed in terms of the reduced temperature  $\epsilon$ :<sup>19</sup>

$$M(\epsilon) \sim D^{-\beta/\nu} \tilde{M}(D^{1/\nu} |\epsilon|). \quad (3)$$

Thus, it is expected that for the optimum set of parameters  $T_c^\infty$ ,  $\beta$ , and  $\nu$ , the  $M(T)$  data for all different particle sizes  $D = 2, \dots, 9$  will collapse onto  $\tilde{M}(x)$  after rescaling the  $M$ -axis by the factor  $D^{\beta/\nu}$  and  $T$ -axis by  $D^{1/\nu} |\epsilon|$ . This is indeed confirmed in Figs. 1(c) and 1(d), which show excellent quality of data scaling for both LE FePt and NE models assuming scaling parameters summarized in Table I. The optimization

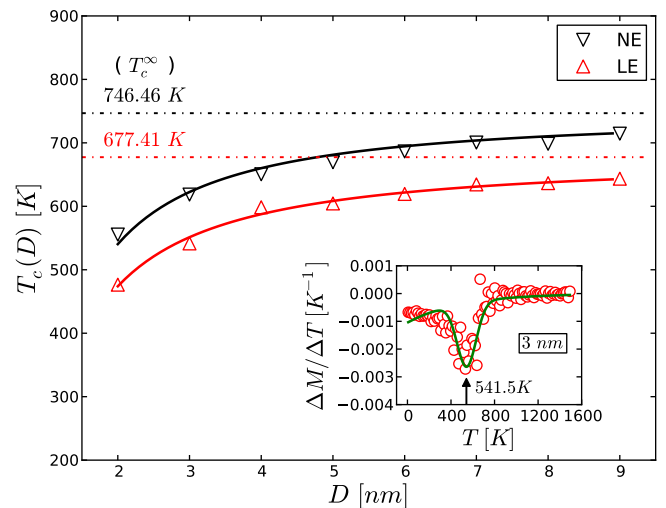


FIG. 2. Dependence of the Curie temperature  $T_c$  on the particle diameter  $D$  for NE and LE FePt systems.  $T_c$  for every  $D$  corresponds to a minimum of the differentiated  $M$  vs  $T$  dependence, as illustrated in the inset for 3 nm LE FePt grain. Solid lines through the triangular points are fits of Eq. (1) with  $d_0$  being the only fit parameter and the bulk  $T_c^\infty$  (dashed lines) and  $\nu$  obtained from the FSS analysis and listed in Table I.

procedure for finding the parameters  $T_c^\infty$ ,  $\beta$ ,  $\nu$  in Table I leading to the best scaling shown in Figs. 1(c) and 1(d) was based on minimizing, in the least-squares sense, the differences between the vertical coordinates of all data points for every  $D$  using the interpolation approach reviewed in Ref. 20.

According to the summary given in Table I, the  $T_c^\infty \sim 677.4 \pm 10.7$  K obtained from the FSS analysis of the LE FePt model data is somewhat smaller than the expected value of 750 K for bulk FePt.<sup>11</sup> However, given that there are no adjustable parameters (all parameters for the FePt Hamiltonian are determined from DFT calculations<sup>8</sup>), the agreement is reasonable. Moreover, according to Ref. 7, the size dependent structural ordering effect not included in the present modeling can result in the increase of  $T_c^\infty$  of the bulk FePt, which might account for the difference. For the NE model, critical exponents agree within the confidence interval with  $\beta = 0.36$  and  $\nu = 0.71$  for the isotropic Heisenberg model<sup>15</sup> which validates the present approach. This also suggests that in the NE case the value of the anisotropy constant  $K_i$  in Eq. (2) is insufficient to induce a crossover to the universality class of the 3D Ising model for which  $\beta = 0.325$  and  $\nu = 0.630$ .<sup>15</sup> For the LE FePt model, the value of the exponent  $\nu$  is slightly higher than in the NE case suggesting that the FePt system might belong to a universality class different from that of the isotropic Heisenberg model. However, more extensive analysis which would allow extraction of a complete spectrum of critical exponents is required to quantify the universality class of FePt system. Such analysis is beyond the scope of the present work.

Having obtained the bulk  $T_c^\infty$ , we now mimic the experimental procedure and fit Eq. (1) to the  $T_c(D)$  data in Fig. 2 with  $d_0$  being the only fit parameter. We fix the phenomenological shift exponent to  $\lambda = \nu^{-1}$  with the values of  $\nu$  as obtained from the FSS analysis in Table I. Fig. 2 shows an excellent agreement between the one-parameter fits of Eq. (1) and the data, with the values of fitted  $d_0$  listed in Table I. The parameter  $d_0$  obtained for LE FePt agrees closely with the experimentally reported value,<sup>11</sup> validating the approach further. We note that in experiments the exponent  $\lambda$  is often considered as a fit parameter as well because  $\nu$  is often unknown and, moreover,  $\lambda$  does not always agree with  $\nu^{-1}$  due to the importance of higher order corrections to finite size scaling which are not included in Eq. (1).<sup>9,12,13</sup> We found that such two-parameters fits of Eq. (1) to our data yield  $\nu = 0.94 \pm 0.03$  and  $d_0 = 0.56 \pm 0.03$  for the NE model,

TABLE I. Critical exponents  $\beta$  and  $\nu$ , and the bulk  $T_c^\infty$  obtained from the FSS analysis according to Eq. (3) for the NE and the LE FePt Hamiltonians. The microscopic length  $d_0$  was obtained by fitting Eq. (1) to the  $T_c$  vs  $D$  dependence obtained by differentiating the  $M$  vs  $T$  data for different sizes  $D$  (Fig. 2). For comparison the experimental data of Ref. 11 and the values for the Heisenberg Hamiltonian<sup>15</sup> are also given.

	NE $\mathcal{H}$	LE-FePt $\mathcal{H}$	Experimental <sup>11</sup>	Heisenberg Hamiltonian <sup>15</sup>
$\beta$	$0.38 \pm 0.03$	$0.33 \pm 0.10$	—	0.36
$\nu$	$0.79 \pm 0.11$	$0.85 \pm 0.10$	$0.91 \pm 0.10$	0.71
$T_c^\infty$ (K)	$746.5 \pm 5.45$	$677.4 \pm 10.66$	$775 \pm 10$	—
$d_0$ (nm)	$0.71 \pm 0.02$	$0.72 \pm 0.02$	$0.84 \pm 0.05$	—

and  $\nu = 0.85 \pm 0.04$  and  $d_0 = 0.72 \pm 0.04$  for the LE FePt model. While the values for the NE model are unrealistically off the expected range for the Heisenberg model probably due to high sensitivity to parameter correlation during the fitting, for the LE FePt model the agreement is remarkable. Hence, the approach based on fixing  $\lambda$  to the bulk value of  $\nu^{-1}$  obtained from the FSS is preferred here.

Now that Eq. (1) has been fully quantified in terms of the parameters  $T_c^\infty$ ,  $\lambda$ , and  $d_0$ , we proceed to analyze the relationship between the distribution functions  $f_T(T_c)$  and  $f_D(D)$ , assuming the realistic scenario of a lognormal distribution of diameter  $f_D(D) = (D\tilde{\sigma}_D\sqrt{2\pi})^{-1} \exp(-(\ln D - \tilde{D})^2 / 2\tilde{\sigma}_D^2)$  with  $\tilde{D}$  and  $\tilde{\sigma}_D^2$  being, respectively, the mean and variance of the random variable  $\ln(D)$ .<sup>21</sup> Given that the dependence  $T_c(D)$  as defined by Eq. (1) is monotonic and that distribution functions  $f_T$  and  $f_D$  are univariate, the transformation law reads  $f_T(T_c) = |D'(T_c)|f_D(D(T_c))$ ,<sup>22</sup> where  $D(T_c)$  is the inverse of Eq. (1) and the prime denotes the derivative  $d/dT_c$ . Thus, rearranging Eq. (1) gives  $D(T_c) = d_0\epsilon_c^{-1/\lambda}$  and  $D'(T_c) = \lambda^{-1}d_0/(T_c^\infty\epsilon_c^{1+1/\lambda})$ , which after algebraic manipulations and using the substitution  $\epsilon_c = (T_c^\infty - T_c)/T_c^\infty$  leads to the expression

$$f_T(\Delta T_c) = \frac{1}{\sqrt{2\pi}\Delta T_c\tilde{\sigma}_T} \exp\left(-\frac{(\ln\Delta T_c - \tilde{T})^2}{2\tilde{\sigma}_T^2}\right), \quad (4)$$

with  $\Delta T_c = T_c^\infty - T_c$ . Equation (4) is a lognormal distribution function with logarithmic mean  $\tilde{T} = \lambda(\ln(d_0(T_c^\infty)^{1/\lambda}) - \tilde{D})$  and variance  $\tilde{\sigma}_T^2 = \lambda^2\tilde{\sigma}_D^2$ . Examples of the distribution functions for both NE and LE FePt models are shown in Fig. 3. It can be seen that the characteristic tail of the lognormal distribution is to low values of  $T_c$ , essentially because of the cut-off imposed by the parameter  $T_c^\infty$ .

In addition to  $\tilde{T}$ ,  $\tilde{\sigma}_T^2$ , and  $\tilde{D}$ ,  $\tilde{\sigma}_D^2$  from the practical point of view, it is also useful to identify the relationship between the arithmetic mean values and variances:  $\langle T_c \rangle$ ,  $\sigma_T^2$ , and  $\langle D \rangle$ ,  $\sigma_D^2$ . Straightforward manipulation of standard expressions relevant to the lognormal distribution<sup>21</sup> gives

$$\frac{\langle T_c \rangle}{T_c^\infty} = 1 - \left(\frac{d_0}{\langle D \rangle}\right)^\lambda \left(1 + \frac{\sigma_D^2}{\langle D \rangle^2}\right)^{(\lambda^2+\lambda)/2}, \quad (5a)$$

$$\frac{\sigma_T^2}{\langle \Delta T_c \rangle^2} = -1 + \left(1 + \frac{\sigma_D^2}{\langle D \rangle^2}\right)^{\lambda^2}. \quad (5b)$$

Equation (5a) reduces to Eq. (1) in the absence of randomness  $\sigma_D \rightarrow 0$ , in which case also  $\sigma_T \rightarrow 0$  in Eq. (5b), as expected. Moreover, given the  $\lambda$  values found here, increasing  $\sigma_D$  results in increase of  $\langle T_c \rangle$  and  $\sigma_T$ .

In conclusion, we have performed a finite size scaling analysis based on the calculated  $M(T)$  data sets for grains of different size  $D$  and extracted the bulk value of Curie temperature and critical exponents. This allows the quantification of the  $T_c(D)$  dependence based on the scaling relation Eq. (1) and identification of the relationship between the  $T_c$  distribution  $f_T(T_c)$  and grain size distribution  $f_D(D)$  as Eq. (4). Equation (4) demonstrates that a lognormal form of the distribution function is preserved under the critical scaling

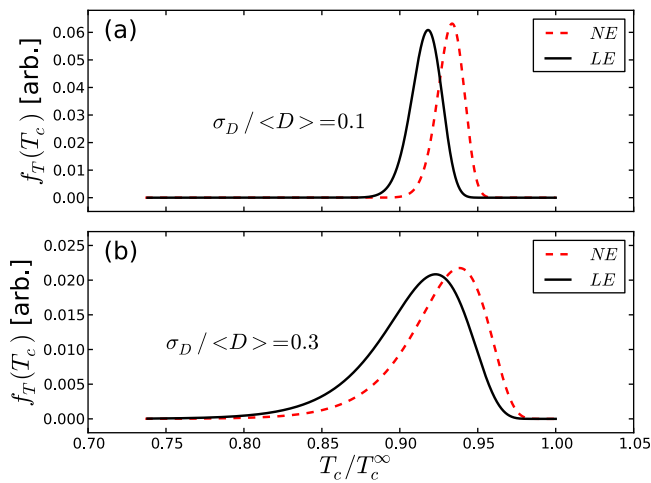


FIG. 3. Distribution function  $f_T(T_c)$  calculated from Eq. (4) for  $\langle D \rangle = 6$  nm and  $\sigma_D/\langle D \rangle = 0.1$  (a) and  $0.3$  (b), for NE and LE FePt models.

Eq. (1). Importantly, we show analytically that standard deviations of  $f_T(T_c)$  and  $f_D(D)$  are related through the shift exponent  $\lambda$  as  $\tilde{\sigma}_T = \lambda \tilde{\sigma}_D$  or, equivalently,  $\sigma_T$  and  $\sigma_D$  through Eq. (5). Consequently,  $\lambda$  is potentially an important physical quantity in relation to HAMR, and one which is expected to be material dependent through the physical concept of universality, as demonstrated here by comparing the long range exchange FePt model with a Heisenberg-like system with short range interaction.

This work was supported by the European Community's Seventh Framework Programme (FP7/2007-2013) under grant agreements NMP3-SL-2008-214469 (UltraMagnetron) and N 214810 (FANTOMAS). O.H. acknowledges support from a Marie Curie Intra European Fellowship within the 7th European Community Framework Programme under grant agreement PIEF-GA-2010-273014 (MENCOFINAS).

- <sup>1</sup>R. E. Rottmayer, S. Batra, D. Buechel, W. A. Challener, J. Hohlfeld, Y. Kubota, L. Li, B. Lu, C. Mihalcea, K. Mountfield, K. Pelhos, C. Peng, T. Rausch, M. A. Seigler, D. Weller, and X. M. Yang, *IEEE Trans. Magn.* **42**, 2417 (2006).
- <sup>2</sup>M. H. Kryder, E. C. Gage, T. W. McDaniel, W. A. Challener, R. E. Rottmayer, G. Ju, Y.-T. Hsia, and M. F. Erden, *Proc. IEEE* **96**, 1810 (2008).
- <sup>3</sup>W. A. Challener, C. Peng, A. V. Itagi, D. Karns, W. Peng, Y. Peng, X. Yang, X. Zhu, N. J. Gokemeijer, Y. T. Hsia, G. Ju, R. E. Rottmayer, M. A. Seigler, and E. C. Gage, *Nat. Photon.* **3**, 220 (2009).
- <sup>4</sup>M. A. Seigler, W. A. Challener, E. Gage, N. Gokemeijer, G. Ju, B. Lu, K. Pelhos, C. Peng, R. E. Rottmayer, X. Yang, H. Zhou, and T. Rausch, *IEEE Trans. Magn.* **44**, 119 (2008).
- <sup>5</sup>N. Kazantseva, D. Hinzke, R. W. Chantrell, and U. Nowak, *Europhys. Lett.* **86**, 27006 (2009).
- <sup>6</sup>J. Barker, R. F. L. Evans, and R. W. Chantrell, D. Hinzke, and U. Nowak, *Appl. Phys. Lett.* **97**, 192504 (2010).
- <sup>7</sup>S. Okamoto, N. Kikuchi, O. Kitakami, and T. Miyazaki, *Phys. Rev. B* **66**, 024413 (2002).
- <sup>8</sup>O. N. Mryasov, U. Nowak, K. Y. Guslienko, and R. W. Chantrell, *Europhys. Lett.* **69**, 805–811 (2005).
- <sup>9</sup>F. Huang, G. J. Mankey, M. T. Kief, and R. F. Willis, *J. Appl. Phys.* **73**, 6760 (1993).
- <sup>10</sup>J. Wang, W. Wu, F. Zhao, and G. Zhao, *Phys. Rev. B* **84**, 174440 (2011).
- <sup>11</sup>Ch. Rong, D. Li, V. Nandwana, N. Poudyal, Y. Ding, Z. L. Wang, H. Zeng, and J. Ping Liu, *Adv. Mater.* **18**, 2984 (2006).
- <sup>12</sup>M. Henkel, S. Andrieu, P. Bauer, and M. Piccuch, *Phys. Rev. Lett.* **80**, 4783 (1998).
- <sup>13</sup>R. Zhang and R. F. Willis, *Phys. Rev. Lett.* **86**, 2665 (2001).
- <sup>14</sup>H. M. Lu, Z. H. Cao, C. L. Zhao, P. Y. Li, and X. K. Meng, *J. Appl. Phys.* **103**, 123526 (2008).
- <sup>15</sup>J. M. Yeomans, *Statistical Mechanics of Phase Transitions* (Oxford University Press, 1992).
- <sup>16</sup>A. Lyberatos and R. W. Chantrell, *J. Appl. Phys.* **73**, 6501 (1993).
- <sup>17</sup>A. Lyberatos, D. V. Berkov, and R. W. Chantrell, *J. Phys.: Condens. Matter* **5**, 8911 (1999).
- <sup>18</sup>K. Binder, *Rep. Prog. Phys.* **60**, 487 (1997).
- <sup>19</sup>N. Goldenfeld, *Lectures on Phase Transitions and the Renormalization Group* (Addison-Wesley, 1992).
- <sup>20</sup>S. M. Bhattarjee and F. Seno, *J. Phys. A* **34**, 6375 (2001).
- <sup>21</sup>In case of lognormal probability distribution  $f(x) = (x\tilde{\sigma}\sqrt{2\pi})^{-1} \exp(-(\ln x - \tilde{\mu})^2/2\tilde{\sigma}^2)$ , logarithmic mean  $\tilde{\mu}$  and variance  $\tilde{\sigma}^2$  are related to arithmetic mean  $\langle x \rangle$  and variance  $\sigma^2$  as  $\exp(\tilde{\mu}) = \langle x \rangle (1 + \sigma^2/\langle x \rangle^2)^{-1/2}$  and  $\exp(\tilde{\sigma}^2) = 1 + \sigma^2/\langle x \rangle^2$  (Ref. 22).
- <sup>22</sup>A. Papoulis and S. U. Pillai, *Probability, Random Variables and Stochastic Processes* (McGraw-Hill, 2002).